Efficient Indirect Interatomic Coulombic Decay Induced by Photoelectron Impact Excitation in Large Pure Helium Nanodroplets

L. Ben Ltaief,[1,*] K. Sishodia,[2] S. Mandal,[3] S. De,[2] S. R. Krishnan,[2] C. Medina,[4] N. Pal,[5] R. Richter,[5] T. Fennel,[6] and M. Mudrich[1,†]

[1]*Department of Physics and Astronomy, Aarhus University, 8000 Aarhus C, Denmark*
[2]*Quantum Center of Excellence for Diamond and Emergent Materials and Department of Physics, Indian Institute of Technology Madras, Chennai 600036, India*
[3]*Indian Institute of Science Education and Research, Pune 411008, India*
[4]*Institute of Physics, University of Freiburg, 79104 Freiburg, Germany*
[5]*Elettra-Sincrotrone Trieste, 34149 Basovizza, Trieste, Italy*
[6]*Institute for Physics, University of Rostock, 18051 Rostock, Germany*

(Received 2 March 2023; accepted 5 June 2023; published 12 July 2023)

Ionization of matter by energetic radiation generally causes complex secondary reactions that are hard to decipher. Using large helium nanodroplets irradiated by extreme ultraviolet (XUV) photons, we show that the full chain of processes ensuing primary photoionization can be tracked in detail by means of high-resolution electron spectroscopy. We find that elastic and inelastic scattering of photoelectrons efficiently induces interatomic Coulombic decay (ICD) in the droplets. This type of indirect ICD even becomes the dominant process of electron emission in nearly the entire XUV range in large droplets with radius $\gtrsim$40 nm. Indirect ICD processes induced by electron scattering likely play an important role in other condensed-phase systems exposed to ionizing radiation as well, including biological matter.

DOI: 10.1103/PhysRevLett.131.023001

Ionization of matter by extreme ultraviolet (XUV) and x-ray radiation involves cascades of secondary processes, including electron scattering, intramolecular relaxation, and intermolecular transfer of charge and energy. These cascades comprise both ultrafast electronic processes and nuclear motion, spanning timescales of femtoseconds up to nanoseconds and beyond. Unraveling the details of such ionization cascades generally is a formidable task due to the high complexity of interactions and the resulting congestion of experimental spectra [1]. However, understanding and even controlling ionization mechanisms in condensed-phase systems, in particular, those producing low-energy electrons that cause radiation damage in biological matter [2,3], is crucial for improving radiotherapies [4]. Here we present a comprehensive study of the ionization mechanisms of a model condensed-phase system—nanometer-sized droplets of helium (He)—by XUV radiation. Owing to the simple electronic structure of the He atom and the peculiar quantum-fluid properties of He nanodroplets, we are able to resolve all primary and secondary ionization processes up to the level of involved excited quantum states and charge states of the products. In particular, we find that both elastic and inelastic electron collisions on He atoms in the droplets efficiently induce further ionizations by interatomic Coulombic decay (ICD) [5,6]. For large He droplets with radius $\gtrsim$40 nm, electron impact-induced ICD even becomes the dominant channel of electron and ion emission.

The most important aspect of ICD is that the energy deposited in one atom or molecule is transferred to another which in turn is ionized. ICD has been characterized in detail for small van der Waals molecules and clusters [7,8]. More recently, the focus has shifted to more relevant condensed-phase systems [9,10], where light-matter interactions are more complex and ICD is harder to decipher; competing processes and electron scattering tend to obscure the signatures of ICD in the measured spectra [11–13]. Variants of ICD have been observed both for pure He droplets and for heterogeneous droplets doped with foreign species. In those experiments, He droplets were resonantly excited or simultaneously ionized and excited by XUV radiation [14–22]. ICD-like processes have also been detected as minor channels in strong-field ionized He droplets and rare-gas clusters, where electron-ion recombination leads to the population of excited atomic states [23–26].

The ICD process reported here is not induced directly by XUV radiation, but rather indirectly by electrons emitted by primary photoionization, subsequently interacting with He atoms of the droplet. We observe it for both pure and doped He droplets in a broad range of photon energies $h\nu > 44$ eV up to the soft x-ray range. While this indirect ICD process is particularly well discernable in He nanodroplets, we believe that it plays an important role in all condensed-phase media subjected to ionizing radiation. In particular, molecular systems such as liquid water tend to form electronically excited states (excitons) by electron-ion

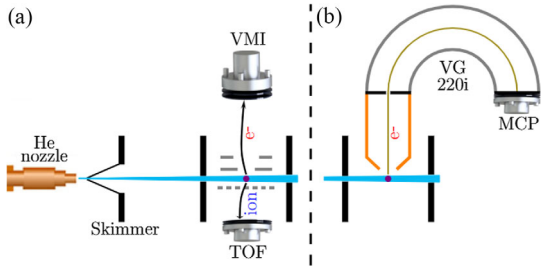

FIG. 1. Sketch of the experimental setups used in this work. (a) He nanodroplet beam source and VMI–time-of-flight (TOF) spectrometer. (b) Hemispherical electron analyzer coupled to a microchannel plate (MCP) detector.

recombination, which subsequently decay by ICD. While excitons have been found to diffuse over large distances in water ice [27], their characteristics and mobility remain poorly understood [28].

For the analysis of secondary processes leading to ICD, we used He nanodroplets and performed two experiments at the GasPhase beamline at the synchrotron radiation facility Elettra, Trieste, Italy. The setups are schematically depicted in Fig. 1. In the first one [Fig. 1(a)], a mobile He droplet apparatus was attached to an electron-ion coincidence velocity-map imaging (VMI) spectrometer [29]. This arrangement has been described before [19,30]. In short, a continuous beam of He nanodroplets containing 10^4 (droplet radius $R = 5$ nm) up to $\sim 10^8$ ($R = 75$ nm) He atoms per droplet is generated by expanding He out of a cryogenic nozzle at a temperature ranging from 16 down to 8 K and 50 bar He backing pressure. A mechanical chopper is used for discriminating all the spectra shown here from the background.

In the detector chamber further downstream, the He droplet beam intersects the XUV beam with flux $\Phi \approx 10^{14}$ s^{-1} cm^{-2} in the VMI spectrometer at right angles. Electron spectra are inferred from electron images by Abel inversion [31]. This setup allows us to simultaneously measure spectra of all emitted electrons and of electrons emitted in coincidence with specific fragment ions in a wide energy range. In the second arrangement [Fig. 1(b)], a hemispherical electron analyzer (VG-220i) mounted at the magic angle is used to measure high-resolution electron spectra.

In addition to these common features present for all droplet sizes, more features appear and grow in the electron spectra when the droplet radius is increased from $R = 5$ nm [red line in Fig. 2(a)] to $R \gtrsim 20$ nm (black line). The salient new feature is a peak around 15 eV, which even surpasses the photoline for large droplets with $R \gtrsim 40$ nm. This peak remains nearly constant in energy for all $h\nu > 45$ eV; see Fig. 2 in the Supplemental Material [32], which includes Refs. [33–45]. Its energy is close to that previously observed in experiments where He droplets were resonantly excited by intense XUV pulses from a free-electron laser

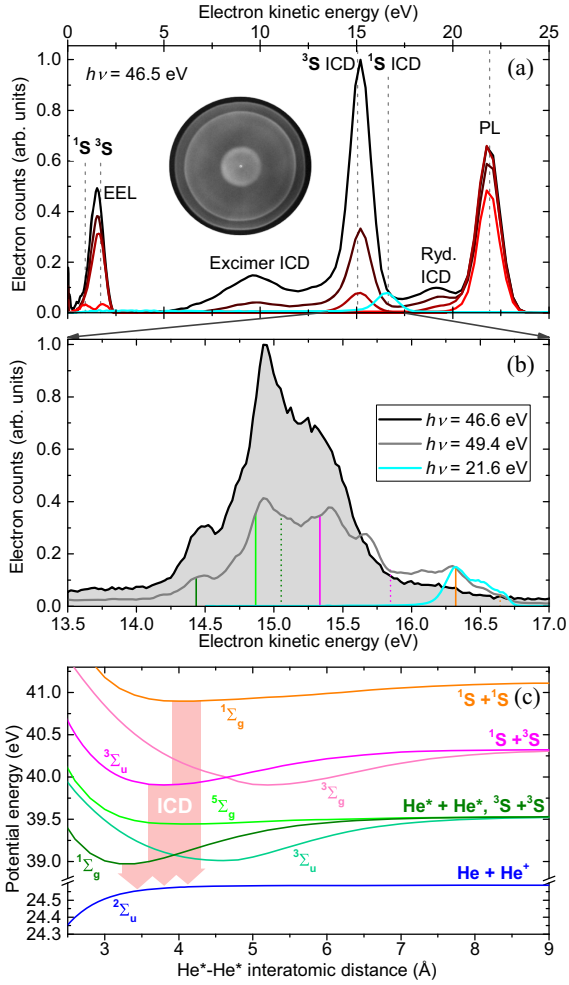

FIG. 2. (a) Electron spectra of variable size measured at various $h\nu$'s and inferred from VMI as that shown in inset ($h\nu = 46.5$ eV, $R = 50$ nm). Red and black lines are spectra of He droplets of radii $R = 5$, 20, 35, and 75 nm (red to black). The cyan line is a reference spectrum at $h\nu = 21.6$ eV and $R = 50$ nm. The vertical dashed lines indicate expected electron energies based on atomic He levels. (b) High-resolution analyzer spectra measured around the main ICD peak for $R = 50$ nm and in the regime of impact excitation (black and gray lines) and resonant excitation (cyan line). The colored stick spectrum indicates characteristic electron energies for ICD of a He*-He* pair formed in ^{3}S and ^{1}S atomic states (dashed lines) and a He*-He* pair forming Σ and Π molecular states (solid lines). The line colors match the potential energy curves involved in the ICD process, shown in (c) [22]. All spectra are normalized to the photon flux and to the $h\nu$-dependent absorption cross section of He.

(FEL) [21,22]. There, multiply excited He droplets decayed by ICD according to the reaction $\mathrm{He}^* + \mathrm{He}^* \longrightarrow \mathrm{He}^+ + \mathrm{He} + e_{\mathrm{ICD}}$ occurring in He droplets [6]. He* stands for an excited He atom in the lowest optically accessible excited $1s2s\ ^1$S state. In fact, when we tune $h\nu$ to the strongest resonance of He droplets at $h\nu = 21.6$ eV ($1s2p\ ^1$P state) in the present synchrotron experiment, we also detect ICD out of the $1s2s\ ^1$S state leading to emission of electrons with

kinetic energy around 16.5 eV [cyan line in Figs. 2(a) and 2(b)]. Although the photon flux is lower than in FEL experiments by orders of magnitude, large He droplets can still be multiply excited owing to their large resonant absorption cross section (25 Mb for each He atom in the droplet, see Supplemental Material, Sec. IV [32] and Ref. [30]). At $h\nu = 46.5$ eV, the absorption cross section of He is only 2.3 Mb [46] and excitation of He requires secondary e-He inelastic collisions that occur with probability < 1. Nevertheless, we detect ICD electrons at $h\nu =$ 46.5 eV with factor 20 higher rate than at $h\nu = 21.6$ eV when taking the $h\nu$-dependent absorption cross section into account. Therefore, we will argue that a different secondary process facilitates the formation of pairs of He^*'s as precursors of ICD: Consecutive e-He impact excitation and elastic scattering of the slowed electron leads to recombination with its parent ion as schematically depicted in Fig. 3(a). This one-photon process is even more efficient than ICD induced by multiple photon absorption by the droplets under the present conditions.

To get more detailed insight into this unusual indirect ICD process, we use the electron analyzer to measure ICD electron spectra with much higher resolution than is possible by the VMI technique [black and gray lines in Fig. 2(b)]. Clearly, the peak structure is more complex than that for ICD after resonant optical excitation ($h\nu = 21.6$ eV, cyan line). There, electrons are mostly produced by decay of pairs of He^*'s in the $^1\Sigma_g$ state correlating to two atoms in $1s2s\ ^1$S singlet states [22]. In contrast, both singlet and triplet states of He e-He can be excited by electron impact. A detailed peak analysis of the high-resolution ICD spectra (Supplemental Material, Fig. 3 [32]) reveals mainly seven peaks, where the dominant ones (labeled as A, B, C) are related to He^*'s in the metastable $1s2s\ ^3$S state. The smaller peaks D, E, F only appear at $h\nu > 46.6$ eV (Supplemental Material, Fig. 4 [32]) and are attributed to ICD involving higher-lying states. We ascribe the dominant role of the $1s2s\ ^3$S state to its long lifetime ~15 μs [45], whereas all higher excited states rapidly decay by droplet-induced relaxation [47,48] and fluorescence emission, including the $1s2s\ ^1$S state [49–53]. Furthermore, the $1s2s\ ^3$S and higher triplet states are populated by autoionization and recombination of $1sns$ excited states with $n \geq 3$ [54].

We conclude that this unusual indirect ICD is a slow process involving the following steps: (i) photoionization followed by photoelectron impact excitation of neutral He, hence formation of He^*, (ii) multiple elastic e-He scattering and electron-ion recombination, (iii) electronic relaxation of the two He^*'s to the lowest excited (mostly triplet) states [48,55], and (iv) ejection of the He^*'s to the droplet surface where they roam until two He^*'s encounter and decay by ICD [56]. The crucial steps and the associated energetics of this ICD process are represented in Fig. 3. Absorption of two photons by the droplets followed by

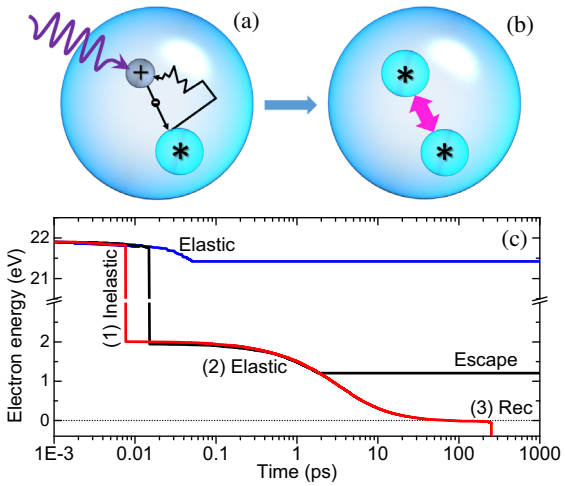

FIG. 3. Illustration of the main ICD mechanism in He droplets induced by photoelectron impact excitation and electron-He^+ recombination (a), leading to two He excitations which subsequently decay by ICD (b). (c) Simulated time evolution of the total energy of a photoelectron in a He droplet of radius $R = 150$ nm at $h\nu = 46.5$ eV for the cases of pure elastic scattering (blue line) and inelastic scattering leading to the escape from the droplet (black line) and to recombination of the electron with its parent ion (red line). The corresponding trajectory in real space is shown in the Supplemental Material, Fig. 10 [32].

electron impact excitation and ICD contributes to a lesser extent.

Additional decay channels are ICD involving He_2^* excimers formed by association of He^*'s with neighboring ground state He atoms and ICD involving a He^* in a highly excited Rydberg state. These processes appear in the electron spectra of Fig. 2(a) around 10 and 19.6 eV, respectively. The latter is only active near the electron impact excitation threshold ($h\nu = 44.5$–46.5 eV, see Supplemental Material, Fig. 5 [32]), where e-He^+ recombination occurs at very low electron energy. Direct evidence for ICD where a He_2^* excimer relaxes to the ground state and a neighboring He^* or He_2^* is ionized is obtained from electron and ion VMI recorded in coincidence with ions and electrons, respectively (see Supplemental Material, Fig. 6 [32]).

Our assertion of the essential role of the one-photon-induced indirect process leading to efficient ICD is further confirmed by measurements of the ICD electron yield as a function of the intensity of radiation, see Supplemental Material, Fig. 8 [32]. At $h\nu = 46.5$ eV we find a power-law dependence with exponent $\alpha = 1.0$ indicating single-photon absorption, whereas for resonant two-photon excitation per droplet at $h\nu = 21.0$ eV we find $\alpha = 1.3$. At $h\nu = 50$ eV, $\alpha = 1.15$ indicating that both one- and two-photon absorption contributes to the ICD signal.

To further establish the multistep mechanism leading to indirect ICD, we performed 3D classical Monte Carlo trajectory simulations of electrons propagating inside He nanodroplets. Binary elastic and inelastic collisions are

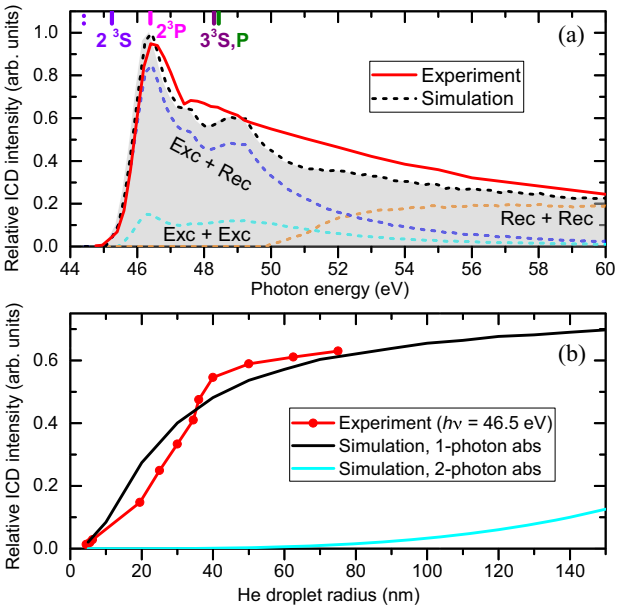

FIG. 4. (a) Experimental and simulated yields of ICD electrons in proportion to photoelectrons as a function of $h\nu$ for He droplets of radius $R = 50$ nm. Colored dashed lines indicate different channels leading to ICD in the simulation. Colored short lines at top scale indicate He excited state energies shifted by 0.84 eV. The vertical violet short dashed line indicates the atomic He electron impact excitation threshold at $h\nu = 44.4$ eV. (b) Relative ICD electron yield as a function of He droplet radius at fixed $h\nu = 46.5$ eV. The solid lines show the simulation for one- and two-photon excitation of the droplets.

taken into account according to the known differential cross sections [57,58] (for details, see Supplemental Material, Secs. IV and V [32]). Figure 3(c) shows the evolution of the total electron energy along three selected trajectories. When the electron undergoes only elastic scattering, it rapidly reaches the droplet surface and escapes with insignificant loss of energy (blue line). However, given the atomic density of He droplets close to that of bulk superfluid He (0.022 $Å^{-3}$), the electron has a high probability of colliding inelastically with a He atom after about 10 fs, thereby suddenly losing ≥ 20.6 eV of its kinetic energy [black and red lines, step (1)]. Subsequently, the electron undergoes multiple elastic collisions with He atoms (2) which leads to a slow, frictionlike damping within about 10 ps. Despite the large mismatch of electron mass and He atomic mass (1/7300), the resulting diffusionlike electron motion can be fully stopped given the large sizes of He droplets $R > 20$ nm we consider here. In this case, it is eventually drawn back to its parent He^+ ion via Coulomb attraction and recombines with it (3) after about 100 ps (red line). Note that these values are in good agreement with previous findings for bulk liquid He [45]. Trajectories where two He^*'s are formed in one droplet by electron impact and by recombination to the $1s2s\,^3S$ state are counted as ICD events.

The simulated numbers of ICD events following one- and two-photon ionization in proportion to the number of directly emitted electrons are shown in Fig. 4(a) as blue, orange, and cyan dashed lines, respectively, for a He droplet of size $R = 50$ nm and for $h\nu$'s tuned across the He impact excitation threshold (see details in the Supplemental Material, Sec. IV [32]). They are summed [black dashed lines in Fig. 4(a)] and compared to the experimental ICD rate normalized to the rate of detected photoelectrons (red solid line). To reproduce the sharp ICD peak around $h\nu = 46.5$ eV, He electron impact excitation energies are shifted by 0.84 eV with respect to atomic-level energies. This shift is consistent with blueshifts of excited states observed in optical and e-He impact excitation spectra [50,59]. The best fit of the simulated and experimental data is obtained when scaling down the channels leading to ICD by electron impact excitation followed by e-He^+ recombination (Rec) [blue dashed lines in Fig. 4(a)] and electron impact ionization followed by recombination of the two emerging electrons [orange dashed line in Fig. 4(a)] by factors 0.3 and 0.1, respectively (see Supplemental Material, Sec. IV [32]).

Overall, the simulation confirms our interpretation that ICD is mainly initiated by one-photon ionization. At $h\nu = 45$–53 eV, impact excitation of He by the photoelectron and e-He^+ recombination is the main pathway to ICD. At $h\nu \gtrsim 53$ eV, the electron impact-ionization cross section exceeds those for electron impact excitation and recombination of two electrons dominates. At $h\nu > 65.4$ eV (not shown), multiple electron impact excitation and ionization can generate two or more He^*'s in a droplet, thereby further enhancing ICD. Two-photon absorption causing the photoemission of two electrons that both impact excite He^*'s in the same droplet only plays a minor role in this droplet size range 5–75 nm, but may become important for larger droplets and higher radiation intensities [16,21].

We point out that this type of ICD is not restricted to pure He droplets; in He droplets doped with lithium (Li) atoms, ICD also occurs between a He^* and a Li atom, thereby creating a Li^+ ion and an ICD electron [20]. The yield of Li^+ ions produced in this way at $h\nu > 44.4$ eV follows essentially the same $h\nu$ dependence (see Supplemental Material, Fig. 9 [32]), highlighting the relevance of this ICD mechanism also for heterogeneous systems.

In conclusion, in large He droplets irradiated by XUV light at $h\nu \gtrsim 44.4$ eV, ICD of pairs of He^*'s formed by electron impact and by electron-ion recombination is an important relaxation mechanism generating electrons with characteristic energy $\approx$15 eV. High-resolution electron spectra reveal that mainly the lowest metastable excited state of He contributes, indicating that higher-lying states relax radiatively and nonradiatively prior to ICD. This sets the timescale for this type of ICD to nanoseconds or even longer. For droplet radii $R \gtrsim 40$ nm, ICD even becomes the dominant electron emission channel. Figure 4(b) shows the experimental and simulated (see Supplemental Material, Sec. IV [32]) yields of ICD electrons normalized to the sum

of all detected electrons as a function of R. Starting at $R \approx 5$ nm, both experimental and simulated ICD electron yields monotonously rise and reach a value of about 0.65 at $R = 75$ nm. We refrain from analyzing larger droplets, as more complex processes will contribute, such as multiphoton absorption [cyan curve in Fig. 4(b)], shadowing, nanofocusing [60], and trapping of electrons at the droplet surface [61]. Future studies should aim at studying the dynamics of this indirect ICD [22,62] and quantifying the role of competing fluorescence decay channels [63]. Comparative studies for other condensed-phase systems should be done to confirm the general relevance of this type of ICD for generating slow electrons, which can cause radiation damage in biological matter [2].

M. M. and L. B. L. acknowledge financial support by Deutsche Forschungsgemeinschaft (Project No. BE 6788/1-1), by the Danish Council for Independent Research Fund (DFF) via Grant No. 1026-00299B, and by the Carlsberg Foundation. We thank the Danish Agency for Science, Technology, and Innovation for funding the instrument center DanScatt. T. F. acknowledges support by the Deutsche Forschungsgemeinschaft (DFG, German Research Foundation) via SFB 1477 "light-matter interactions at interfaces" (Project No. 441234705) and via the Heisenberg program (Project No. 436382461). S. R. K. thanks the Department of Science and Technology, Government of India, for support through the DST-DAAD scheme and Science and Engineering Research Board. S. R. K. acknowledges support for this research through the Indo-French Center for Promotion of Advanced Research (CEFIPRA). S. R. K., K. S., and S. D. acknowledge the support of the Scheme for Promotion of Academic Research Collaboration, Ministry of Education, Government of India, and the Institute of Excellence program at IIT-Madras via the Quantum Center for Diamond and Emergent Materials. S. R. K. gratefully acknowledges support of the Max Planck Society's Partner group program, and M. M. and S. R. K. acknowledge funding from the SPARC program, MHRD, India. The research leading to this result has been supported by the project CALIPSOplus under Grant Agreement No. 730872 from the EU Framework Programme for Research and Innovation HORIZON 2020 and by the COST Action CA21101 "Confined Molecular Systems: From a New Generation of Materials to the Stars (COSY)".

*Corresponding author.
ltaief@phys.au.dk
†Corresponding author.
mudrich@phys.au.dk

[1] V. Stumpf, K. Gokhberg, and L. S. Cederbaum, The role of metal ions in x-ray-induced photochemistry, Nat. Chem. **8**, 237 (2016).
[2] E. Alizadeh, T. M. Orlando, and L. Sanche, Biomolecular damage induced by ionizing radiation: The direct and indirect effects of low-energy electrons on DNA, Annu. Rev. Phys. Chem. **66**, 379 (2015).
[3] B. Boudaïffa, P. Cloutier, D. Hunting, M. A. Huels, and L. Sanche, Resonant formation of DNA strand breaks by low-energy (3 to 20 eV) electrons, Science **287**, 1658 (2000).
[4] L. Sanche, Interaction of low energy electrons with DNA: Applications to cancer radiation therapy, Radiat. Phys. Chem. **128**, 36 (2016).
[5] L. S. Cederbaum, J. Zobeley, and F. Tarantelli, Giant Intermolecular Decay and Fragmentation of Clusters, Phys. Rev. Lett. **79**, 4778 (1997).
[6] A. I. Kuleff, K. Gokhberg, S. Kopelke, and L. S. Cederbaum, Ultrafast Interatomic Electronic Decay in Multiply Excited Clusters, Phys. Rev. Lett. **105**, 043004 (2010).
[7] U. Hergenhahn, Interatomic and intermolecular Coulombic decay: The early years, J. Electron Spectrosc. Relat. Phenom. **184**, 78 (2011).
[8] T. Jahnke, U. Hergenhahn, B. Winter, R. Dorner, U. Fruhling, P. V. Demekhin, K. Gokhberg, L. S. Cederbaum, A. Ehresmann, A. Knie *et al.*, Interatomic and intermolecular Coulombic decay, Chem. Rev. **120**, 11295 (2020).
[9] X. Ren, E. Wang, A. D. Skitnevskaya, A. B. Trofimov, K. Gokhberg, and A. Dorn, Experimental evidence for ultrafast intermolecular relaxation processes in hydrated biomolecules, Nat. Phys. **14**, 1062 (2019).
[10] P. Zhang, C. Perry, T. T. Luu, D. Matselyukh, and H. J. Wörner, Intermolecular Coulombic Decay in Liquid Water, Phys. Rev. Lett. **128**, 133001 (2022).
[11] D. Iablonskyi *et al.*, Slow Interatomic Coulombic Decay of Multiply Excited Neon Clusters, Phys. Rev. Lett. **117**, 276806 (2016).
[12] L. Ben Ltaief, A. Hans, P. Schmidt, X. Holzapfel, F. Wiegandt, P. Reiss, C. Küstner-Wetekam, T. Jahnke, R. Dörner, A. Knie *et al.*, VUV photon emission from Ne clusters of varying sizes following photon and photoelectron excitations, J. Phys. B **51**, 065002 (2018).
[13] S. Malerz, F. Trinter, U. Hergenhahn, A. Ghrist, H. Ali, C. Nicolas, C.-M. Saak, C. Richter, S. Hartweg, L. Nahon *et al.*, Low-energy constraints on photoelectron spectra measured from liquid water and aqueous solutions, Phys. Chem. Chem. Phys. **23**, 8246 (2021).
[14] D. S. Peterka, J. H. Kim, C. C. Wang, and D. M. Neumark, Photoionization and photofragmentation of SF_6 in helium nanodroplets, J. Phys. Chem. B **110**, 19945 (2006).
[15] C. C. Wang, O. Kornilov, O. Gessner, J. H. Kim, D. S. Peterka, and D. M. Neumark, Photoelectron imaging of helium droplets doped with Xe and Kr atoms, J. Phys. Chem. **112**, 9356 (2008).
[16] Y. Ovcharenko *et al.*, Novel Collective Autoionization Process Observed in Electron Spectra of He Clusters, Phys. Rev. Lett. **112**, 073401 (2014).
[17] M. Shcherbinin, A. C. LaForge, V. Sharma, M. Devetta, R. Richter, R. Moshammer, T. Pfeifer, and M. Mudrich, Interatomic Coulombic decay in helium nanodroplets, Phys. Rev. A **96**, 013407 (2017).
[18] F. Wiegandt, F. Trinter, K. Henrichs, D. Metz, M. Pitzer, M. Waitz, E. Jabboura al Maalouf, C. Janke, J. Rist,

N. Wechselberger, T. Miteva, S. Kazandjian, M. Schöffler, N. Sisourat, T. Jahnke, and R. Dörner, Direct observation of interatomic Coulombic decay and subsequent ion-atom scattering in helium nanodroplets, Phys. Rev. A **100**, 022707 (2019).

[19] D. Buchta, S. R. Krishnan, N. B. Brauer, M. Drabbels, P. O'Keeffe, M. Devetta, M. Di Fraia, C. Callegari, R. Richter, M. Coreno, K. C. Prince, F. Stienkemeier, R. Moshammer, and M. Mudrich, Charge transfer and penning ionization of dopants in or on helium nanodroplets exposed to EUV radiation, J. Phys. Chem. A **117**, 4394 (2013).

[20] L. Ben Ltaief, M. Shcherbinin, S. Mandal, S. Krishnan, A. LaForge, R. Richter, S. Turchini, N. Zema, T. Pfeifer, E. Fasshauer *et al.*, Charge exchange dominates long-range interatomic Coulombic decay of excited metal-doped helium nanodroplets, J. Phys. Chem. Lett. **10**, 6904 (2019).

[21] Y. Ovcharenko, A. LaForge, B. Langbehn, O. Plekan, R. Cucini, P. Finetti, P. O'Keeffe, D. Iablonskyi, T. Nishiyama, K. Ueda *et al.*, Autoionization dynamics of helium nanodroplets resonantly excited by intense XUV laser pulses, New J. Phys. **22**, 083043 (2020).

[22] A. C. LaForge *et al.*, Ultrafast Resonant Interatomic Coulombic Decay Induced by Quantum Fluid Dynamics, Phys. Rev. X **11**, 021011 (2021).

[23] B. Schütte, M. Arbeiter, T. Fennel, G. Jabbari, A. Kuleff, M. Vrakking, and A. Rouzée, Observation of correlated electronic decay in expanding clusters triggered by intense near-infrared fields, Nat. Commun. **6**, 8596 (2015).

[24] T. Oelze, B. Schütte, M. Müller, J. P. Müller, M. Wieland, U. Frühling, M. Drescher, A. Al-Shemmary, T. Golz, N. Stojanovic *et al.*, Correlated electronic decay in expanding clusters triggered by intense XUV pulses from a free-electron-laser, Sci. Rep. **7**, 40736 (2017).

[25] M. Kelbg, M. Zabel, B. Krebs, L. Kazak, K.-H. Meiwes-Broer, and J. Tiggesbäumker, Auger emission from the Coulomb explosion of helium nanoplasmas, J. Chem. Phys. **150**, 204302 (2019).

[26] M. Kelbg, M. Zabel, B. Krebs, L. Kazak, K.-H. Meiwes-Broer, and J. Tiggesbäumker, Temporal Development of a Laser-Induced Helium Nanoplasma Measured through Auger Emission and Above-Threshold Ionization, Phys. Rev. Lett. **125**, 093202 (2020).

[27] N. G. Petrik and G. A. Kimmel, Electron-Stimulated Reactions at the Interfaces of Amorphous Solid Water Films Driven by Long-Range Energy Transfer from the Bulk, Phys. Rev. Lett. **90**, 166102 (2003).

[28] B. C. Garrett, D. A. Dixon, D. M. Camaioni, D. M. Chipman, M. A. Johnson, C. D. Jonah, G. A. Kimmel, J. H. Miller, T. N. Rescigno, P. J. Rossky *et al.*, Role of water in electron-initiated processes and radical chemistry: Issues and scientific advances, Chem. Rev. **105**, 355 (2004).

[29] P. O'Keeffe, P. Bolognesi, M. Coreno, A. Moise, R. Richter, G. Cautero, L. Stebel, R. Sergo, L. Pravica, Y. Ovcharenko, and L. Avaldi, A photoelectron velocity map imaging spectrometer for experiments combining synchrotron and laser radiations, Rev. Sci. Instrum. **82**, 033109 (2011).

[30] D. Buchta, S. R. Krishnan, N. B. Brauer, M. Drabbels, P. O'Keeffe, M. Devetta, M. Di Fraia, C. Callegari, R. Richter, M. Coreno, K. C. Prince, F. Stienkemeier, J. Ullrich, R. Moshammer, and M. Mudrich, Extreme ultraviolet ionization of pure He nanodroplets: Mass-correlated photoelectron imaging, penning ionization, and electron energy-loss spectra, J. Chem. Phys. **139**, 084301 (2013).

[31] B. Dick, Inverting ion images without Abel inversion: Maximum entropy reconstruction of velocity maps, Phys. Chem. Chem. Phys. **16**, 570 (2014).

[32] See Supplemental Material at http://link.aps.org/supplemental/10.1103/PhysRevLett.131.023001 for additional experimental data (electron energy-loss spectra, high-resolution ICD electron spectra including a peak analysis, electron-ion coincidence spectra including ion kinetic energy distributions, intensity-dependent ICD-yield measurements, ICD measurements for doped he nanodroplets) and a more detailed description of the numerical simulation.

[33] K. von Haeften, T. Laarmann, H. Wabnitz, T. Möller, and K. Fink, Size and isotope effects of helium clusters and droplets: Identification of surface and bulk-volume excitations, J. Phys. Chem. **115**, 7316 (2011).

[34] S. Kazandjian *et al.*, Frustrated Coulomb explosion of small helium clusters, Phys. Rev. A **98**, 050701(R) (2018).

[35] A. Mauracher, O. Echt, A. Ellis, S. Yang, D. Bohme, J. Postler, A. Kaiser, S. Denifl, and P. Scheier, Cold physics and chemistry: Collisions, ionization and reactions inside helium nanodroplets close to zero K, Phys. Rep. **751**, 1 (2018).

[36] M. Shcherbinin, A. C. LaForge, M. Hanif, R. Richter, and M. Mudrich, Penning ionization of acene molecules by helium nanodroplets, J. Phys. Chem. A **122**, 1855 (2018).

[37] R. J. LeRoy and G. T. Kraemer, BCONT 2.2. Computer program for calculating absorption coefficients, emission intensities or (golden rule) predissociation rates. The source code and manual for this program may be obtained from "computer programs" link at http://leroy.uwaterloo.ca, University of Waterloo Chemical Physics Research, Report No. CP-650R2 (2004).

[38] S. L. Fiedler and J. Eloranta, Interaction of helium Rydberg state atoms with superfluid helium, J. Low Temp. Phys. **174**, 269 (2014).

[39] B. E. Callicoatt, K. Förde, L. F. Jung, T. Ruchti, and K. C. Janda, Fragmentation of ionized liquid helium droplets: A new interpretation, J. Chem. Phys. **109**, 10195 (1998).

[40] X. Sheng, J. P. Toennies, and K. T. Tang, Conformal Analytical Potential for All the Rare Gas Dimers over the Full Range of Internuclear Distances, Phys. Rev. Lett. **125**, 253402 (2020).

[41] A. Carrington, C. H. Pyne, and P. J. Knowles, Microwave electronic spectrum of the He_2^+ ion, J. Chem. Phys. **102**, 5979 (1995).

[42] M. Adibzadeh and C. E. Theodosiou, Elastic electron scattering from inert-gas atoms, At. Data Nucl. Data Tables **91**, 8 (2005).

[43] U. Henne and J. P. Toennies, Electron capture by large helium droplets, J. Chem. Phys. **108**, 9327 (1998).

[44] D. Golden and H. Bandel, Absolute total electron-helium-atom scattering cross sections for low electron energies, Phys. Rev. **138**, A14 (1965).

[45] D. N. McKinsey, C. R. Brome, S. N. Dzhosyuk, R. Golub, K. Habicht, P. R. Huffman, E. Korobkina, S. K. Lamoreaux, C. E. H. Mattoni, A. K. Thompson, L. Yang, and J. M. Doyle,

Time dependence of liquid-helium fluorescence, Phys. Rev. A **67**, 062716 (2003).
[46] J. Samson and W. C. Stolte, Precision measurements of the total photoionization cross-sections of He, Ne, Ar, Kr, and Xe, J. Electron Spectrosc. Relat. Phenom. **123**, 265 (2002).
[47] M. Mudrich and F. Stienkemeier, Photoionisaton of pure and doped helium nanodroplets, Int. Rev. Phys. Chem. **33**, 301 (2014).
[48] J. D. Asmussen *et al.*, Unravelling the full relaxation dynamics of superexcited helium nanodroplets, Phys. Chem. Chem. Phys. **23**, 15138 (2021).
[49] J. W. Keto, F. J. Soley, M. Stockton, and W. A. Fitzsimmons, Dynamic properties of neutral excitations produced in electron-bombarded superfluid helium. II. Afterglow fluorescence of excited helium molecules, Phys. Rev. A **10**, 887 (1974).
[50] M. Joppien, R. Karnbach, and T. Möller, Electronic Excitations in Liquid Helium: The Evolution from Small Clusters to Large Droplets, Phys. Rev. Lett. **71**, 2654 (1993).
[51] K. von Haeften, T. Laarmann, H. Wabnitz, and T. Möller, Observation of Atomiclike Electronic Excitations in Pure ^{3}He and ^{4}He Clusters Studied by Fluorescence Excitation Spectroscopy, Phys. Rev. Lett. **87**, 153403 (2001).
[52] K. von Haeften, T. Laarmann, H. Wabnitz, and T. Möller, Bubble Formation and Decay in ^{3}He and ^{4}He Clusters, Phys. Rev. Lett. **88**, 233401 (2002).
[53] D. N. McKinsey, C. R. Brome, S. N. Dzhosyuk, R. Golub, K. Habicht, P. R. Huffman, E. Korobkina, S. K. Lamoreaux, C. E. H. Mattoni, A. K. Thompson, L. Yang, and J. M. Doyle, Time dependence of liquid-helium fluorescence, Phys. Rev. A **67**, 062716 (2003).
[54] K. von Haeften, A. R. B. de Castro, M. Joppien, L. Moussavizadeh, R. von Pietrowski, and T. Möller, Discrete Visible Luminescence of Helium Atoms and Molecules Desorbing from Helium Clusters: The Role of Electronic, Vibrational, and Rotational Energy Transfer, Phys. Rev. Lett. **78**, 4371 (1997).
[55] M. Mudrich, A. LaForge, A. Ciavardini, P. O'Keeffe, C. Callegari, M. Coreno, A. Demidovich, M. Devetta, M. Di Fraia, M. Drabbels *et al.*, Ultrafast relaxation of photoexcited superfluid he nanodroplets, Nat. Commun. **11** (2020).
[56] H. Buchenau, J. P. Toennies, and J. A. Northby, Excitation and ionization of ^{4}He clusters by electrons, J. Chem. Phys. **95**, 8134 (1991).
[57] D. F. Register, S. Trajmar, and S. K. Srivastava, Absolute elastic differential electron scattering cross sections for He: A proposed calibration standard from 5 to 200 eV, Phys. Rev. A **21**, 1134 (1980).
[58] Y. Ralchenko, R. Janev, T. Kato, D. Fursa, I. Bray, and F. de Heer, Electron-impact excitation and ionization cross sections for ground state and excited helium atoms, At. Data Nucl. Data Tables **94**, 603 (2008).
[59] M. Shcherbinin, F. V. Westergaard, M. Hanif, S. Krishnan, A. LaForge, R. Richter, T. Pfeifer, and M. Mudrich, Inelastic scattering of photoelectrons from He nanodroplets, J. Chem. Phys. **150**, 044304 (2019).
[60] L. Ban, B. L. Yoder, and R. Signorell, Photoemission from free particles and droplets, Annu. Rev. Phys. Chem. **71**, 315 (2020).
[61] M. Fárník, U. Henne, B. Samelin, and J. P. Toennies, Differences in the Detachment of Electron Bubbles from Superfluid ^{4}He Droplets versus Nonsuperfluid ^{3}He Droplets, Phys. Rev. Lett. **81**, 3892 (1998).
[62] M. P. Ziemkiewicz, D. M. Neumark, and O. Gessner, Ultrafast electronic dynamics in helium nanodroplets, Int. Rev. Phys. Chem. **34**, 239 (2015).
[63] K. von Haeften, T. Laarmann, H. Wabnitz, and T. Möller, Relaxation dynamics of ^{3}He and ^{4}He clusters and droplets studied using near infrared and visible fluorescence excitation spectroscopy, Phys. Chem. Chem. Phys. **25**, 1863 (2023).